



**HAL**  
open science

## Wind-tunnel experiments on atmospheric heavy gas dispersion: Metrological aspects

Cristina Vidali, Massimo Marro, Horacio Correia, Louis Gostiaux, Simon Jallais, Deborah Houssin, Elena Vyazmina, Pietro Salizzoni

### ► To cite this version:

Cristina Vidali, Massimo Marro, Horacio Correia, Louis Gostiaux, Simon Jallais, et al.. Wind-tunnel experiments on atmospheric heavy gas dispersion: Metrological aspects. *Experimental Thermal and Fluid Science*, 2022, 130, pp.110495. 10.1016/j.expthermflusci.2021.110495 . hal-03429564

**HAL Id: hal-03429564**

**<https://hal.science/hal-03429564>**

Submitted on 29 Nov 2022

**HAL** is a multi-disciplinary open access archive for the deposit and dissemination of scientific research documents, whether they are published or not. The documents may come from teaching and research institutions in France or abroad, or from public or private research centers.

L'archive ouverte pluridisciplinaire **HAL**, est destinée au dépôt et à la diffusion de documents scientifiques de niveau recherche, publiés ou non, émanant des établissements d'enseignement et de recherche français ou étrangers, des laboratoires publics ou privés.

# Wind-tunnel experiments on atmospheric heavy gas dispersion: metrological aspects

Cristina Vidali<sup>a,b,\*</sup>, Massimo Marro<sup>a</sup>, Horacio Correia<sup>a</sup>, Louis Gostiaux<sup>a</sup>, Simon Jallais<sup>b</sup>, Deborah Houssin<sup>b</sup>, Elena Vyazmina<sup>b</sup>, Pietro Salizzoni<sup>a</sup>

<sup>a</sup>*Univ Lyon, Ecole Centrale de Lyon, CNRS, Univ Claude Bernard Lyon 1, INSA Lyon, LMFA, UMR5509, 69130, Ecully, France*

<sup>b</sup>*Air Liquide Paris Research & Development Center, Paris Innovation Campus, 1 chemin de la Porte des Loges, Les Loges-en-Josas, Jouy-en-Josas, France.*

---

## Abstract

We propose a new experimental protocol to investigate the atmospheric dispersion of a dense gas in wind-tunnel experiments. Simultaneous measurements of concentration and velocity are performed by coupling a flame ionization detector (FID) and a hot-wire anemometer (HWA), whose probes are located sufficiently close to each other so that the respective measurements **correspond** to a same sampling volume. The heavy gas emission consists in a mixture of air, carbon dioxide, and ethane. Carbon dioxide is used as a buoyant agent, and ethane is used as a tracer, its concentration being detected by the FID. In this context, the main metrological issue of the setup concerns the response of the FID and the HWA to different proportions of the two gases in the mixture. Notably, the presence of carbon dioxide affects the linear response of the FID, which can attain a saturation level, as well as the response of the HWA, due to the varying density of the gas. This can be compensated by determining a non-linear calibration curve of the FID, which is used to determine the instantaneous fluid density, and to apply a time-dependent correction to the HWA response. To analyse the performances of the coupled HWA-FID system we realised wind-tunnel experiments of tracer dispersion in a turbulent boundary layer. The estimate of mass fluxes through different sections downwind the source enlightens the reliability of the experimental results, and show that the measurements within a negatively buoyant gas plume are as

---

\*Corresponding author

*Email address: cristina.vidali@ec-lyon.fr (Cristina Vidali)*

accurate as those within a passive scalar plume.

*Keywords:* Calibration, hot-wire anemometry, flame ionization detector, wind tunnel, heavy gas dispersion

---

## 1. Introduction

Experimental studies in atmospheric wind tunnels still play a major role for our understanding of the physics of pollutant dispersion. Furthermore, these studies provide reference datasets, that can be subsequently used to validate and improve numerical models. The large majority of the experiments performed so far concerned the case of passive (neutrally buoyant) releases, but relatively few studies focused on the case of buoyant gases. Therefore, there is a clear need to improve the characterisation of turbulent fluctuations and mass fluxes within dense gas plumes [1], which requires combined statistics of instantaneous concentration and velocity.

The experimental investigation of the turbulent dispersion of buoyant releases can be performed in both wind tunnels and water flumes. However, the latter are not suited for the simulation of releases characterised by large density differences with the ambient fluid. Indeed, as enlightened by Meroney [2], experiments using salt as a density ingredient can be hardly performed with density differences exceeding 10%. We will therefore focus here only on wind-tunnel experiments, in which gases with molecular weight higher than that of air are employed for the simulation of heavy gas releases.

Combined statistics of concentration and velocity can be actually acquired adopting suitable measurement techniques. Different systems have been developed and employed in wind-tunnel experiments, involving techniques for the measurements of velocity as the hot-wire anemometry (HWA) and the laser Doppler anemometry (LDA). Measurements of scalar concentrations include instead the photo ionization detector (PID), the cold film/wire, and the flame ionization detector (FID).

The HWA [3] is a well established technique, widely employed to measure fluctuating fluid velocities. The calibration procedure is well defined in isodensity flows, but is more complicated for gases with varying density [4, 5, 6, 7, 8]. In order to measure the velocity in gas mixtures (in isothermal conditions), Corrsin [9] combined the cali-

27 brations of HWA obtained for each gas. However, this method led to systematic errors  
28 in the estimate of the coefficients of the calibration King's equation. Pitts and McCaf-  
29 frey [6] calibrated the hot-wire and film anemometers in different gases and defined an  
30 empirical correction of the calibration parameters as a function of the Reynolds ( $Re$ )  
31 and Nusselt ( $Nu$ ) numbers. Wasan and Baid [5] focused on the HWA response in a  
32 carbon dioxide-air mixture, by performing a calibration in pure [gases](#), and then used a  
33 linear [approximation](#) to estimate velocities. All these methods are characterised by a  
34 considerable uncertainty, especially when the two components have molecular weights  
35 significantly different one to the other [7]. McQuaid and Wright [10] examined the  
36 response of HWA in gas mixtures, defining an empirical relation between the molal  
37 concentration of the second component gas mixture and the voltage response. The  
38 main result of this study was the empirical correction on the response of HWA in pres-  
39 ence of gases other than air. A different approach was proposed by Talbot et al. [11].  
40 They performed neon-doping in a variable-viscosity flows of propane-air mixture, and  
41 showed the hot-wire response to be insensitive to the concentration field. Zhu et al.  
42 [12] analysed velocity and turbulence within the dense gas plumes by using hot-film  
43 anemometry with an optimum overheat ratio that allowed them to perform measure-  
44 ments in a range of carbon dioxide ( $CO_2$ ) concentration (less than 25%) that did not  
45 affect the probe sensitivity. Over the range of 0.3-1.1 m/s, the errors in the mean  
46 wind speeds were generally less than 5%. Finally, Banerjee and Andrews [7] per-  
47 formed a detailed procedure to investigate helium-air mixture with HWA, employing  
48 a multiposition-multioverheat hot-wire technique to estimate both velocity and density  
49 fluctuations and defining a calibration surface in function of density and velocity.

50 Coupled measurements of velocity and concentration were most commonly per-  
51 formed with a HWA-FID or HWA-PID system, with the exceptions of Raupach and  
52 Legg [13] and Stapountzis et al. [14], who employed the HWA and a cold wire to mea-  
53 sure the velocity and scalar field, respectively (since they simulated the scalar source  
54 with a heated wire). Fackrell and Robins [15] measured with HWA-FID the first two  
55 moments of the concentration field of a passive scalar plume and estimated the turbu-  
56 lent mass fluxes induced by a point source of varying size and height in a turbulent  
57 boundary layer. Koeltzsch [16] used the same technique to estimate the turbulent mass

58 fluxes in a similar set-up, focusing on the dependence of the turbulent Schmidt number  
59 on the distance from the wall. Metzger and Klewicki [17] developed a sensor combin-  
60 ing HWA with a PID. Talluru et al. [18] used this same system to investigate passive  
61 scalar dispersion in a turbulent boundary layer.

62 Others studies used a coupled system of LDA-FID to directly estimate turbulent  
63 fluxes of a passive scalar [19, 20, 21]. Employing the LDA [22] for the velocity mea-  
64 surements prevents any calibration uncertainty related to a varying density difference,  
65 but may imply other complications. Notably, the aerosols used to seed the flow may af-  
66 fect the concentration statistics measured by the FID. To analyse these and other metro-  
67 logical aspects of these coupled measurements techniques, Marro et al. [23] compared  
68 the HWA-FID and the LDA-FID systems, notably concerning the optimal distance be-  
69 tween the probes (which was found to be equal to 4 mm, i.e.  $0.2L$ , being  $L$  the Eulerian  
70 integral length scale), the evaluation of the time lag (16 ms) of the measured signals  
71 of concentration and velocity, the effect of the seeding on the concentration statistics  
72 for the LDA-FID coupled system. [After having defined](#) the optimal settings of the  
73 probes, they enlightened the reliability of both systems for simultaneous measuring  
74 of high-frequency signals of velocity and concentration in a turbulent boundary layer.  
75 This study showed also that the computations of the cross-correlations between veloc-  
76 ity and scalar fields with two different methods - slot correlation technique [24, 25] and  
77 sample-and-hold reconstruction and resampling - were in good agreement [23].

78 It is worth noting that these coupled techniques have not been used so far to in-  
79 vestigate the dispersion of heavy gas releases. To that purpose, the release of a heavy  
80 gas can be conveniently produced by a mixture of air and carbon dioxide [26, 27, 28,  
81 29, 30, 31]. The local density within the turbulent flow can then be evaluated by a di-  
82 rect estimate of the heavy gas concentration [26, 32] or, alternatively, by adding a tiny  
83 quantity of a gas tracer, whose presence can be detected with a FID. Common tracers  
84 are propane [33] and ethane ( $C_2H_6$ ) [27, 12, 31]. Schatzmann et al. [27] and Donat  
85 and Schatzmann [34] used a gas-probe sampling system connected to a FID to analyse  
86 time averaged concentrations and velocities of heavy gas plumes. Robins et al. [33]  
87 collected simultaneously 16 air samples using a vacuum system and analysed it with a  
88 FID, to estimate the mean concentration field in neutral turbulent boundary layer. They

89 used two additional channels for the calibration, one to determine the background hy-  
90 drocarbon concentration in the wind tunnel and the other to obtain the sensor response  
91 of the calibration gas of known and certified composition. Britter and Snyder [31] mea-  
92 sured with a FID the time averaged concentration field induced by a steady emission  
93 of a passive scalar and a heavy gas. They calibrated the FID using an ethane-air mix-  
94 ture and investigated separately the response of the FID to ethane-air-carbon dioxide  
95 mixture, and corrected the measurements accordingly. Zhu et al. [12] investigated a  
96 ground-level emission of heavy gas, using ethane as tracer and  $CO_2$  as heavy gas, im-  
97 posing a ratio between carbon dioxide and ethane  $r = C_{CO_2}/C_{C_2H_6} = 33.3$ . Moreover,  
98 they tested the response of the FID to ethane-air and ethane-air-carbon dioxide mix-  
99 tures in a series of measurements, in which the source mixtures were diluted with air at  
100 constant rates in a dilution chamber. The same method was employed by Snyder [28].  
101 Recently, Robins et al. [35] performed wind-tunnel experiments of non-buoyant and  
102 dense gas dispersion in complex geometries providing a data set for the mean concen-  
103 tration in the framework of the MODITIC project.

104 This work is part of a project that aims at studying heavy gas dispersion from an  
105 elevated-point source in a turbulent atmospheric boundary layer. Following the recent  
106 works of Iacobello et al. [36] and Marro et al. [23] on passive scalar emissions, we use  
107 a coupled system of HWA-FID to investigate the release of a dense mixture of air,  $CO_2$ ,  
108 and ethane. The aim of the present study is to define a calibration procedure for both  
109 the FID and the HWA that takes into account the influence of the mixture density on  
110 the measuring instruments. In this new approach, the instantaneous measurements of  
111 concentration are used to provide a time-dependent correction of the HWA response.  
112 In this way, we could extend former studies on turbulent dispersion of passive scalars  
113 to the case of negatively buoyant releases. This method allows high-frequency simul-  
114 taneous measurements of velocity and concentration to be performed within heavy gas  
115 plume and, therefore, it opens new perspectives for the investigation of the dynamics  
116 of dense gas dispersion in the atmosphere.

117 In what follow, we first present the experimental setup used for the calibration and  
118 the wind-tunnel experiments (Section 2.1). We continue by describing the character-  
119 istics of the instruments (Section 2.2 and 2.3) and the coupled measurement system

120 (Section 2.4). The calibration procedures are detailed for the FID (Section 3) and the  
121 HWA (Section 4). Finally, we present results on the concentration mean field and the  
122 mean, turbulent, and total mass fluxes estimated over cross-wind sections, verifying the  
123 conservation of the mass within the plume and, therefore, the reliability of the coupled  
124 measurement technique (Section 5).

## 125 **2. Experimental methods**

### 126 *2.1. Experimental setup*

127 The experiments are conducted in the atmospheric wind tunnel of the Laboratoire  
128 de Mécanique des Fluides et d'Acoustique (LMFA) at the École Centrale de Lyon  
129 in France. The recirculating wind tunnel is 14 m long, 3.7 m wide, and 2 m high  
130 with an adjustable ceiling to control pressure gradients. The temperature in the test  
131 section is regulated to limit the temperature variation during a one-day experiment in  
132 the range  $\pm 0.5^\circ\text{C}$ . The wind-tunnel temperature - in a range between  $21^\circ\text{C}$  and  $26^\circ\text{C}$   
133 - is chosen to minimise the temperature difference between the emitted gases (coming  
134 from pressurised bottles) and the wind-tunnel flow.

135 In order to calibrate the instruments, a mixture of air, ethane, and carbon dioxide  
136 is used to generate density controlled gas mixtures. Ethane is employed as a tracer  
137 as the FID is sensitive to its concentration [37]. Ethane has almost the same density  
138 of air ( $\rho_a$ ), while the density of  $\text{CO}_2$  is about  $1.5\rho_a$ . Different fractions of carbon  
139 dioxide are used to modify the density of the gas mixture during the calibration and  
140 the experiments. The mixture device is composed by three different lines (Figure 1),  
141 one for each gas. Every line is equipped with a digital mass-flow controller (Alicat  
142 Scientific MC-Series) that integrates a proportional–integral–derivative controller and  
143 provides the volumetric flow rate  $Q_v$  for each gas. The mass-flow controllers work in a  
144 range between 1 and 20 Nl/min for  $\text{CO}_2$  and air, and between 0.50 and 200 Nml/min for  
145 ethane. The error on the mass-flow rate is estimated by comparison with measurements  
146 provided by a volumetric counter. The maximal difference between the measurements  
147 of the two instruments does not exceed  $\pm 3\%$  [38]. Between the  $\text{CO}_2$  tank and the flow-  
148 meter is placed a heater, to avoid the presence of condensed  $\text{CO}_2$  droplets that could

149 change the dynamics of the dispersion and the response of the instruments. All the lines  
150 are connected to a valve in which gases are blended together before being directed to  
151 the source, as shown in Figure 1. The concentrations of ethane and  $CO_2$  at the source  
152 are computed in volumetric ppm, and referred to as  $c_s = Q_v/Q_{v,s}$ , where  $Q_v$  is the flow  
153 rate of the considered gas and  $Q_{v,s}$  the total flow rate at the source, expressed in l/min.

154 The steady releases of a heavy gas and a passive scalar are investigated in a neu-  
155 tral turbulent boundary layer characterised by free-stream velocity  $U_\infty = 1.45$  m/s and  
156 height  $\delta = 0.8$  m. The turbulent boundary layer is generated by combining the effects  
157 of spires and wall roughness, as described in Nironi et al. [38]. The plume is released  
158 from a metallic stack of internal diameter  $d_s = 0.012$  m and placed at  $h_s = 0.076$  m  
159 from ground level and at  $7.5\delta$  from the beginning of the working section, where the  
160 boundary layer can be considered fully developed (Figure 1). The heavy gas release  
161 is a mixture of air, ethane, and  $CO_2$ , whereas the passive scalar plume consists of an  
162 air-ethane mixture. The sampling duration is 300 s, allowing the stochastic uncertainty  
163 of the concentration statistics (due to the finite size of the sampling) to be of order 0.1  
164 % [38]. The flow rate at the source is  $Q_{v,s} = 16.0$  NI/min for both heavy and passive  
165 releases, corresponding to a vertical velocity of  $w_s = 2.37$  m/s. For the heavy gas emis-  
166 sion the volume flow of  $CO_2$  is 14.8 NI/min, which corresponds to a density at the  
167 source  $\rho_s \approx 1.78$  kg/m<sup>3</sup> (depending on the temperature in the wind tunnel) and to a  
168 relative density difference  $\Delta\rho_s/\rho_a = (\rho_s - \rho_a)/\rho_a \approx 50\%$ .

## 169 2.2. Concentration measurements

170 Concentration is measured with the FID Cambustion HFR400 system, consisting  
171 of a module for hydrocarbon sampling and an electronic control unit [39], that is sen-  
172 sitive to the presence of hydrocarbons [37]. The gas sample is sucked and burned in  
173 the combustion chamber where a cathode collects ions. The instrument returns the  
174 electric potential difference induced by the ionization current, proportional to the num-  
175 ber of atoms of carbon in the gas tracer sampling. The complex combustion process  
176 produces a series of chemical reactions that occur in the combustion chamber. The  
177 presence in the sample of gases other than the tracer, such as  $CO_2$ , influences these  
178 reactions, changing the instrument response. We fix the ratio  $r = C_{CO_2}/C_{C_2H_6}$  between

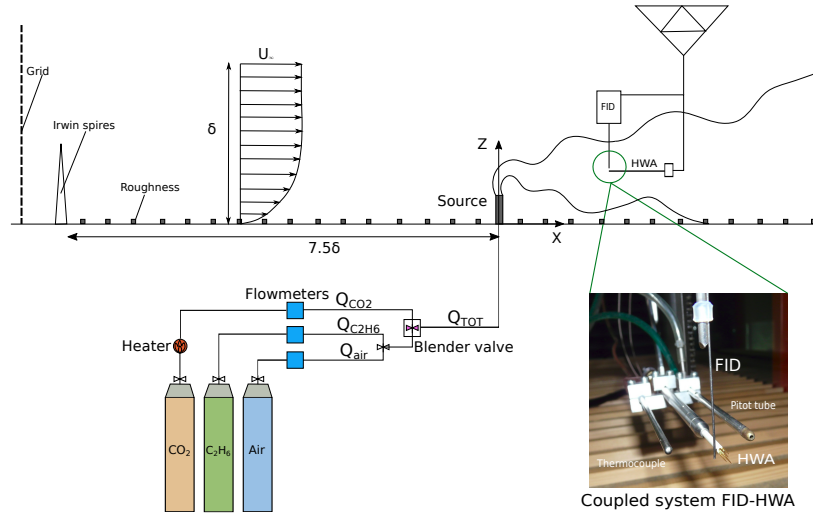


Figure 1: Experimental setup of gas lines and coupled measurements system

179 carbon dioxide and ethane concentration at the source and we assume that  $r$  is constant  
 180 all along the dispersion process. This is justified by the fact that molecular diffusion  
 181 coefficient in air for  $CO_2$  and ethane are comparable  $D_{CO_2} = 1.61 \times 10^{-4} \text{ m}^2/\text{s}$  and  
 182  $D_{C_2H_6} = 1.48 \times 10^{-4} \text{ m}^2/\text{s}$  at 20 °C [40] and that the gases are well blended at the  
 183 emission. The FID is equipped with a sampling tube 0.3 m long and a diameter of  
 184 0.125 mm. Its frequency response is approximately 400 Hz [23].

185 Since the experiments are performed in a recirculating wind tunnel, the increase of  
 186 background concentration over time has to be taken into account. We therefore measure  
 187 the background concentration before and after the registration of each concentration  
 188 time series, we perform a linear interpolation and, finally, we subtract the interpolated  
 189 values from the signal.

### 190 2.3. Velocity measurements

191 Velocity measurements are performed with X-wire probe HWA at constant tem-  
 192 perature [41, 42], of Dantec Dynamics (Streamline 90N10 Frame, with CTA Module  
 193 90C10). The platinum probe wire is 1 mm long and with a diameter of  $5 \mu\text{m}$  and is  
 194 connected to one arm of a Wheatstone bridge. Its velocity-vector acceptance angle is  
 195  $45^\circ$ . In our setup, the HWA has a frequency response of about 5000 Hz. The yaw

196 calibration is not performed. After the calibration procedure, described in Section 4,  
197 we apply a yaw correction with constant coefficients  $k_1^2 = k_2^2 = 0.0225$  to decompose  
198 velocities from the X-probe into longitudinal and transverse velocity components [43].  
199 Since the HWA response is influenced by the  $CO_2$  concentration, it is necessary to  
200 know the instantaneous value of this concentration in the sampling volume to correct  
201 the HWA response. This is made possible through the coupled HWA-FID measurement  
202 system.

#### 203 2.4. Coupled measurement system HWA-FID

204 A coupled HWA-FID system requires the setting of an optimal distance between the  
205 two probes so that these are: i) sufficiently far to avoid any perturbation on the response  
206 of one instrument on the other, and ii) sufficiently close to consider measurements as  
207 performed in the same sampling volume [23]. According to the analysis presented in  
208 Marro et al. [23] this distance is set to 5 mm.

209 In proximity of the coupled HWA-FID system, we install a Pitot-static tube and a  
210 thermocouple monitoring, respectively, the flow velocity and the air temperature during  
211 the experiment. The Pitot-static tube provides a verification of the (time averaged)  
212 longitudinal velocity provided by the HWA measurements, whereas the thermocouple  
213 allows us to check that the temperature inside the wind tunnel is constant ( $\pm 0.5^\circ\text{C}$ )  
214 during the sampling. This is an important requirement to perform HWA measurements  
215 without the need of re-calibrating the instrument [43].

216 The sampling frequency for coupled measurements (HWA and FID) is set at 1000  
217 Hz. Signals of concentration are shifted in time by 16 ms with respect to velocity,  
218 which is the time required for the gas sample to reach the FID combustion chamber  
219 [23]. Once time shifted, the signals do not need resampling and we can compute the  
220 cross statistics.

221 According to the measurements of Nironi et al. [38], the experimental error, esti-  
222 mated by repeating the measurements in a fixed reference location, is 2% for the mean  
223 and the standard deviation of the velocity, and 3% for the mean and the standard devia-  
224 tion of the concentration. With a similar experimental setup, Marro et al. [23] assessed  
225 similar values for the LDA-FID system. Both studies were however performed with

226 passive scalar releases.

### 227 **3. FID calibration in the presence of $CO_2$**

228 The calibration is performed by connecting the output of a three lines mixture  
229 device to a pipe of diameter 0.005 m, with a temperature in the test section in the  
230 range 21-26°C. The FID is placed at the exit of this pipe and we investigated the re-  
231 sponse of the probe for different mixtures of  $CO_2$  and ethane. Figure 2a shows the  
232 response of FID, in volt  $E(V)$ , as a function of the ethane concentration, for different  
233 ratio  $r = C_{CO_2}/C_{C_2H_6}$  of the gas mixture. We note that  $E(V)$  decreases as the ratio  
234  $r$  increases. This means that, for a constant  $C_{C_2H_6}$ , the presence of  $C_{CO_2}$  reduces the  
235 voltage response. Secondly, for pure ethane or low value of  $r$ , it is possible to define  
236 the ethane concentration as a one-to-one function of volts provided by the FID ( $r = 36$   
237 in Figure 2a). As  $C_{CO_2}$  increases ( $r \geq 75$ ), a saturation of the signal occurs and the  
238 relation between  $E(V)$  and  $C_{C_2H_6}$  is no longer one-to-one. The calibration curves col-  
239 lapse on a single curve when the products between  $E(V)$  and the ratio  $r$  are plotted  
240 versus the density of the mixture  $\rho$  (Figure 2b). This analysis allows us to identify a  
241 unique critical density  $\rho_c = 1.56 \text{ kg/m}^3$  in the whole range of values of  $r$  (red line in  
242 Figure 2b), corresponding to 58% of  $CO_2$ . Measurements performed in a mixture with  
243 density  $\rho < \rho_c$  are, therefore, calibrated with a one-to-one function. Since we impose  
244 a constant plume density  $\rho_s > \rho_c$  at the stack, we cannot perform measurements very  
245 close to the source due to the saturation of FID and, therefore, we have to carefully  
246 choose the minimal sampling distance from the release point. We could check that at  
247  $X = 0.250\delta$  the dispersion process ensured that the condition  $\rho < \rho_c$  was fulfilled.

248 To avoid FID saturation, we impose  $50 < r < 60$  for measurements close to the  
249 source, and  $12 < r < 30$  for measurements in the far field. As a general rule, FID  
250 calibration is performed twice a day during the whole experimental campaign.

### 251 **4. HWA Calibration in $CO_2$ -air mixtures**

252 When performing the HWA calibration, the standard procedure determines the sen-  
253 sitivity coefficients of the two wires with respect to different flow variables [3]. This

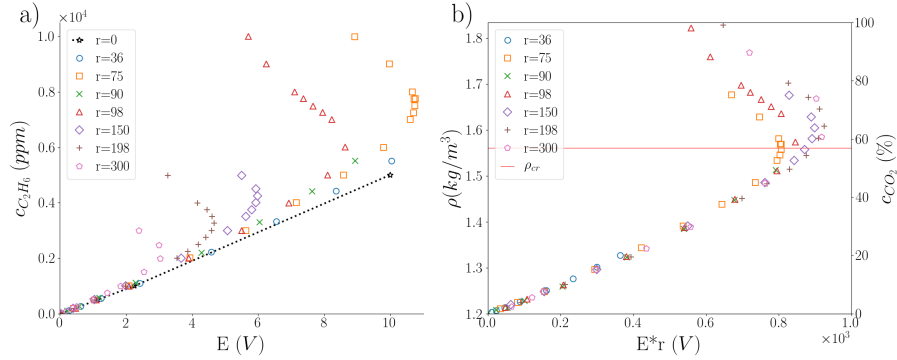


Figure 2: FID calibration curves for varying  $r = C_{CO_2}/C_{C_2H_6}$ . a) Ethane concentration as a function of volt response  $E$  (the dotted line refers to the case of pure ethane). b) Normalized gas-mixture density as a function of  $rE$ .

254 relation depends on velocity, ambient temperature, and gas-mixture density. Here, we  
 255 are particularly concerned with the effect of a varying density on the HWA response.  
 256 In this study, we use a similar approach to that used by Banerjee and Andrews [7] for  
 257 the HWA calibration in the context of a heavy gas atmospheric dispersion. The main  
 258 conceptual difference between our work and the one of Banerjee and Andrews [7] is  
 259 that we use this calibration to perform simultaneous and distinct measurements of con-  
 260 centration and velocity. As already stated, the temperature in the test section of the  
 261 wind tunnel is kept constant during one experiment, but the HWA calibration needs to  
 262 be repeated every time the temperature varies more than  $\pm 0.5^\circ C$ . The calibration of  
 263 the hot-wire anemometer is performed at the exhaust of a pipe of 25 mm in diameter  
 264 and 700 mm long. We use a gas mixture of  $CO_2$  and air with five different ratios of  
 265 the mixture, between 0 and 100%. The procedure includes a velocity correction using  
 266 Pitot-static tube measurements, to take into account the difference between the veloc-  
 267 ity at the centre of the profile of the turbulent flow in the pipe and the average velocity  
 268 over the tube section, as estimated by the flow-meters. From the measurements with  
 269 the Pitot-static tube, we identify a 3rd degree polynomial linking the flow rate and the  
 270 velocity in the range 0 to 3 m/s, that is the velocity range in the experiments. The  
 271 velocity  $U$  is reported in Figure 3a as a function of the volt response  $E_1$ , each set cor-  
 272 responding to a different percentage of carbon dioxide. These data can be fitted by a

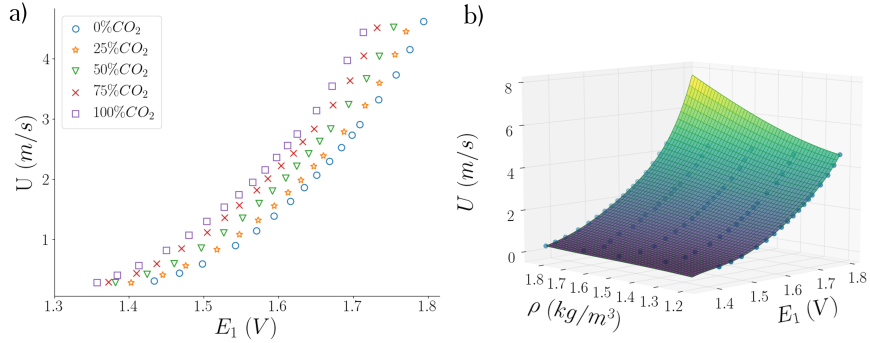


Figure 3: a) HWA calibration curves for gas mixture with increasing quantities of  $CO_2$ : velocities vs volt response. b) HWA calibration surface velocities vs volt response and gas-mixture density.

273 bi-dimensional function that takes into account the dependence of the velocity on both  
 274  $E_1$  (V) and  $\rho$  (Figure 3b). The surface is a polynomial fit of 5th (for  $E_1$ ) and 4th (for  $\rho$ )  
 275 degree of the form  $U(\rho, E_1) = \sum_{i=0}^5 \sum_{j=0}^4 p_{ij} E_1^i \rho^j$ , where the coefficients  $p_{ij}$  are set  
 276 for each calibration. The maximal discrepancies between the fit surface and the actual  
 277 measurements is equal to 2.7% and occurs for small velocities (notably for  $U = 0.58$   
 278 m/s), namely due to the uncertainties related to the flow-meters. In order to use the cal-  
 279 ibration surface  $U(\rho, E_1)$  for instantaneous velocity measurements, the coupled system  
 280 is essential. The estimates of the instantaneous concentrations provided by the FID al-  
 281 low us to evaluate the instantaneous density of the fluid and thus convert accordingly  
 282 the HWA volt response.

## 283 5. Measurements and analysis

284 We investigate the steady release of a heavy gas and a passive scalar in a neutral  
 285 turbulent boundary layer (Section 2.1), performing simultaneous measurements of con-  
 286 centration and velocity profiles downwind the source with the coupled system HWA-  
 287 FID. For each measurement section we measure two profiles: a vertical profile on the  
 288 plume axis ( $y=0$ ) and a transverse profile at a varying vertical height, corresponding  
 289 to that of the maximum value of the mean concentration, as identified in the vertical  
 290 profile.

To compare the results we employ dimensionless concentration and velocities. The latter are denoted as  $u^*$ ,  $w^*$ ,  $v^*$  and are re-scaled by the free-stream velocity  $U_\infty$ . The non-dimensional concentration  $c^*$  is instead normalised as:

$$c^* = c \frac{U_\infty \delta^2}{Q_s} \quad (1)$$

291 In Figure 4 is reported the normalised time averaged concentration, referred to as  
 292  $\bar{c}^*$ , for a heavy gas plume and a passive scalar, i.e. neutral density emission. Each  
 293 profile corresponds to a section at increasing distances from the source. We observe  
 294 that, as  $\bar{c}^*$  decreases downstream the source, the heavy gas plume develops close to  
 295 the ground and it is deflected, due to the negative buoyancy effects. We reported in  
 296 the upper  $x$ -axis the relative averaged density difference, defined as  $\Delta\bar{\rho}/\rho_a = (\bar{\rho} -$   
 297  $\rho_a)/\rho_a$ . The larger density differences are of course observed close to the source.  
 298 The maximal averaged density difference across the first measurement section ( $X/\delta =$   
 299  $0.25$ ) is slightly less than 3%, about 1.5% at the second section, and further reduced  
 300 away from the source. These averaged values are considerably smaller than the typical  
 301 range of density differences over which the FID has been calibrated. Note however  
 302 that the aforementioned averaged values are computed on highly intermittent signals,  
 303 in which peak instantaneous values can be more than 10 times larger than the mean  
 304 value. Since the calibration curve is not linear (in presence of  $CO_2$ ), this latter has to  
 305 be applied to instantaneous concentrations. These features highlight the need for an  
 306 accurate calibration procedure to obtain reliable concentration statistics.

307 Employing our coupled measurement system, adjusted with the HWA and the FID  
 308 calibration, we can also obtain simultaneous measurements of concentration and ve-  
 309 locity, that allow us to measure vertical profiles of streamwise turbulent mass fluxes,  
 310 referred to as  $\overline{u'c'^*}$ , reported in Figure 5a in dimensionless values. As for  $\bar{c}^*$ , the inten-  
 311 sity of  $\overline{u'c'^*}$  decreases with increasing distance from the source as the plume spreads.  
 312 The vertical displacement of the plume has also a role on the spatial evolution of  $\overline{u'c'^*}$ ,  
 313 for the heavy gas emission. Close to the source, the dispersion dynamics is signif-  
 314 icantly influenced by the emission conditions: the source momentum and buoyancy  
 315 alter the velocity field, resulting in values of  $\overline{u'c'^*}$  at the plume centre that are lower for  
 316 the heavy gas plume ( $\approx -7$ ), compared to those observed for the passive scalar release

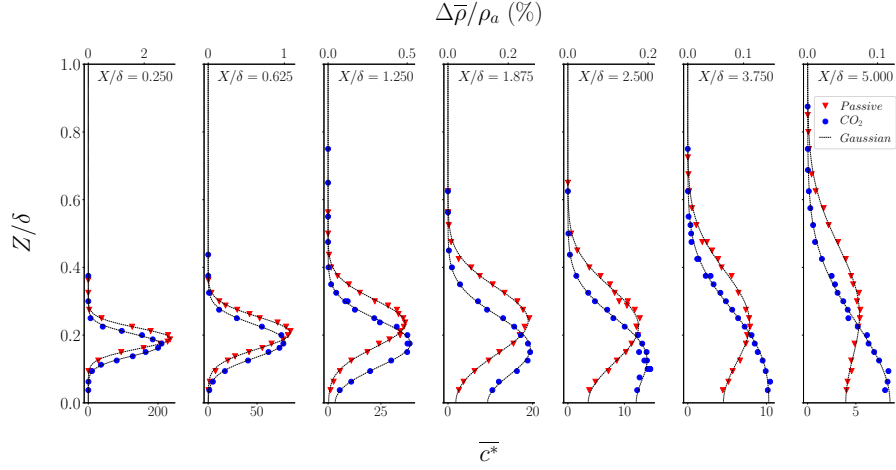


Figure 4: Vertical profiles of the normalized time averaged concentration  $\bar{c}^*$  and relative density difference  $\Delta\bar{\rho}/\rho_a$  at increasing distance from the source for passive (red) and heavy (blue) gas plumes.

317 ( $\approx -5$ ). Moving further away from the source, the peak values of the horizontal turbu-  
 318 lent mass fluxes are similar for the passive and heavy gas, and the mass fluxes gradients  
 319 are progressively smoothed. The profiles present a vertical displacement strictly related  
 320 to the different trajectory of the plume, as showed in Figure 4.

321 We estimate the vertical profiles of the longitudinal time-averaged mass fluxes as  
 322 the product between the mean concentration and mean velocity profiles (Figure 5b).  
 323 The general trend follows that previously observed for the mean concentration profiles  
 324 (Figure 4), with the heavy gas plume deflected towards the ground. Furthermore, near  
 325 the source, the maximum of the streamwise mean mass fluxes is slightly lower for the  
 326 heavy gas plume compared to the passive one. For increasing distance from the source,  
 327 the maximum values of  $\bar{u}^* \cdot \bar{c}^*$  are higher in case of heavy gas release.

In order to evaluate the reliability of our measurements, we have verified the mass  
 conservation downwind the source, by comparing the integrated mass flux at different  
 cross-flow sections,  $Q(x)$ , to the mass-flow rate  $Q_s$  released at the source location, i.e.:

$$\frac{Q}{Q_s} = \int \int \bar{u} \bar{c}^* dy^* dz^*, \quad (2)$$

328 where  $y^* = y/\delta$  and  $z^* = z/\delta$ .

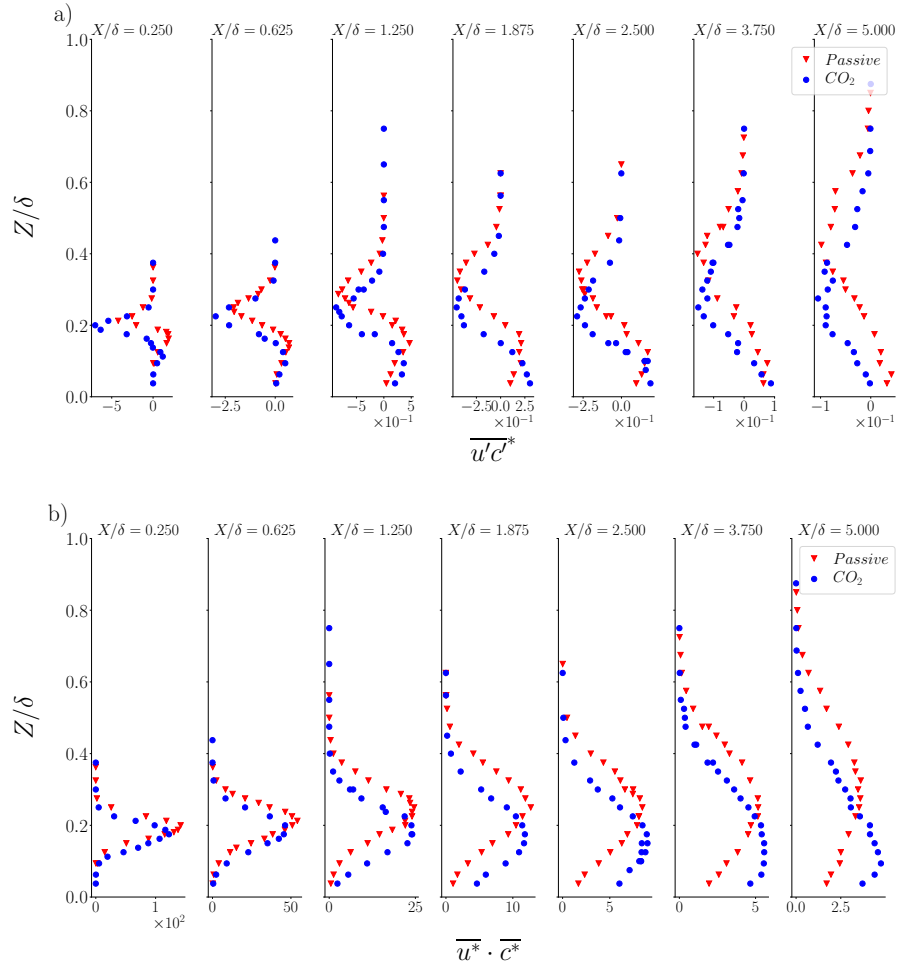


Figure 5: Vertical profiles of a) normalized longitudinal turbulent mass fluxes and b) normalised longitudinal mean mass fluxes for sections at increasing distance from the source for passive and heavy gas plume.

Adopting the Reynolds decomposition, the mass fluxes can be expressed as the sum of the mean and the fluctuating component:

$$\overline{uc^*} = \overline{u^*}(z) \cdot \overline{c^*}(x, y, z) + \overline{u'c'^*}(x, y, z). \quad (3)$$

329 The available information on  $\overline{c^*}(x, y, z)$  and  $\overline{u'c'^*}(x, y, z)$  are limited on the vertical  
 330 and transverse profiles, crossing at the plume centre. To evaluate the mass fluxes on  
 331 the entire cross-section, some hypotheses have to be made. Concentration profiles  
 332 are fitted with a Gaussian function for the transverse profiles and a double symmetric  
 333 Gaussian profile in the vertical direction (to take into account the reflection of the  
 334 plume to the ground). We assume a velocity profile homogeneous in the horizontal  
 335 plane, whereas the dependence on the distance from the wall follows a classical power-  
 336 law (see Nironi et al. [38]). For the turbulent mass fluxes  $\overline{u'c'^*}$ , we linearly fit the  
 337 measured vertical profiles and assume a Gaussian for the transverse profiles, since the  
 338 information collected from the measurements were not sufficient to estimate a more  
 339 specific shape. Despite the large number of approximations adopted to estimate the  
 340 total mass flux, we believe that this procedure provides a useful check of the reliability  
 341 of the experimental results.

342 In Figure 6 we plot  $Q/Q_s$  as a function of the longitudinal distance from the source  
 343 (Figure 6). Similar comparisons were performed by Raupach and Legg [13] and, more  
 344 recently, by Marro et al. [23] in the case of passive emissions. Raupach and Legg [13]  
 345 evaluated the streamwise heat flux induced by an elevated linear source, obtaining val-  
 346 ues with a range of variation up to 20%, with a clearly decreasing trend for increasing  
 347 distances from the source. As pointed out by the authors, this decreasing trend was  
 348 due to the heat losses at the lateral walls of the wind tunnel. Marro et al. [23] analysed  
 349 instead the case of a chemical tracer emitted from a ground-line source and observed a  
 350 global uncertainty on  $Q/Q_s$  of about 8%, that did not depend on the distance from the  
 351 source. Since we use here the same measurement techniques (and same instruments)  
 352 used by Marro et al. [23], we adopt as a reference the same uncertainty for the mass  
 353 fluxes, and therefore we plot 8% error bars in the estimates presented in Figure 6.

354 As Figure 6 shows, the total fluxes  $Q/Q_s$  for both the passive and the heavy gas re-  
 355 lease are slightly underestimated. The discrepancies with the reference value  $Q/Q_s = 1$

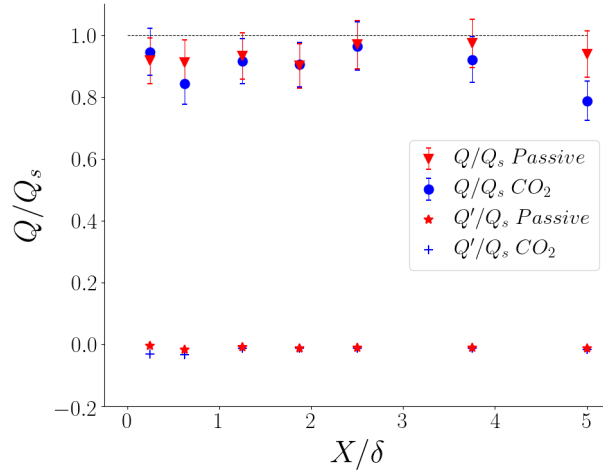


Figure 6: Integrated flux over transverse sections normalized by the flow rate at the source  $Q_s$ , for increasing distance from the source.

356 never exceed 20% and are on average approximately 10%. Of course, these differences  
 357 between our estimates and the reference value are here larger than those observed by  
 358 Marro et al. [23]. This is due to the fact that we are here dealing with a 3D plume,  
 359 whose structure is reconstructed by fitting two profiles only. Instead, the 2D plume  
 360 examined by Marro et al. [23] could be fully characterised by a single profiles of ve-  
 361 locity and concentration statistics (at each downstream location). However, note that  
 362 the discrepancies between our estimates and the reference value  $Q/Q_s = 1$  are very  
 363 similar for the passive scalar and the heavy gas release. We can therefore assert that  
 364 our measurements in the heavy gas plume are as reliable as those performed within a  
 365 passive scalar plume.

366 In Figure 6 we also report the normalized fluctuation fluxes ( $Q'/Q_s$ ), which are  
 367 shown to be negative. Their values are low and they contribute for less than 2% to  
 368 the total mass flux, a value which is systematically lower than that estimated by Marro  
 369 et al. [23] for a line ground-level source. This difference can be explained by noting  
 370 that, when the plume is elevated,  $\overline{u'c'^*}$  has opposite signs above and below the plume  
 371 centreline (as it can be inferred from Figure 5a). Once the plume becomes ground  
 372 based,  $\overline{u'c'^*}$  becomes instead purely negative.

373 In Figure 7 we compare the non-dimensional mass fluxes in the cross-flow section  
374 for heavy gas (Figure 7a, c, e, and g) and passive scalar (Figure 7b, d, f, and h) releases  
375 at increasing distance from the source, with contour values that span from  $10^{-3}$  to  $10^2$ .  
376 The distribution of the mass flux in the different sections confirms what was highlighted  
377 in the previous paragraphs: due to the negative buoyancy the trajectory of the plume is  
378 deflected more rapidly toward the ground compared to the passive scalar plume.

## 379 6. Conclusions

380 We have defined a procedure to calibrate a coupled system of HWA-FID in order  
381 to measure velocity and concentration statistics within heavy gas plumes. This system  
382 provides high-frequency simultaneous concentration and velocity values in the same  
383 sampling volume. The heavy gas mixture was composed by  $CO_2$ , air, and  $C_2H_6$ , the  
384 latter used as a tracer, since its concentration was detected by the FID. The presence of  
385  $CO_2$  in the mixture alters the voltage response of both instruments. For this reason, we  
386 have analysed the FID response as a function of the ratio  $r = C_{CO_2}/C_{C_2H_6}$  and of the  
387 mixture density, identifying a critical density that corresponds to the 58% of  $CO_2$  in  
388 the mixture and thus a value of  $\Delta\rho_c/\rho_a = (\rho_c - \rho_a)/\rho_a \approx 30\%$ . For a mixture density  
389 lower than this value, we could define a one-to-one function to calibrate the FID. The  
390 HWA response depends on both the flow velocity and the density of the gas mixture.  
391 We have therefore defined a procedure to estimate a calibration surface accounting for  
392 the dependence on both quantities.

393 This method is affected by some shortcomings. Notably, we are limited to heavy  
394 gas clouds whose  $CO_2$  peak-concentration does not have to exceed 58%, in order to  
395 calibrate the FID with a one-to-one function. Furthermore, we need to carefully fix the  
396 ratio between carbon dioxide and gas tracer. In particular, we impose a high  $r$  value  
397 close to the source to prevent FID saturation, whereas we adopt releases with a lower  
398  $r$  in order to perform measurements in the far field, so that the ethane concentration is  
399 high enough to be detectable with the FID.

400 As a demonstration, we employed the coupled system HWA-FID in wind-tunnel ex-  
401 periments, simulating a passive scalar and a heavy gas release from an elevated stack.

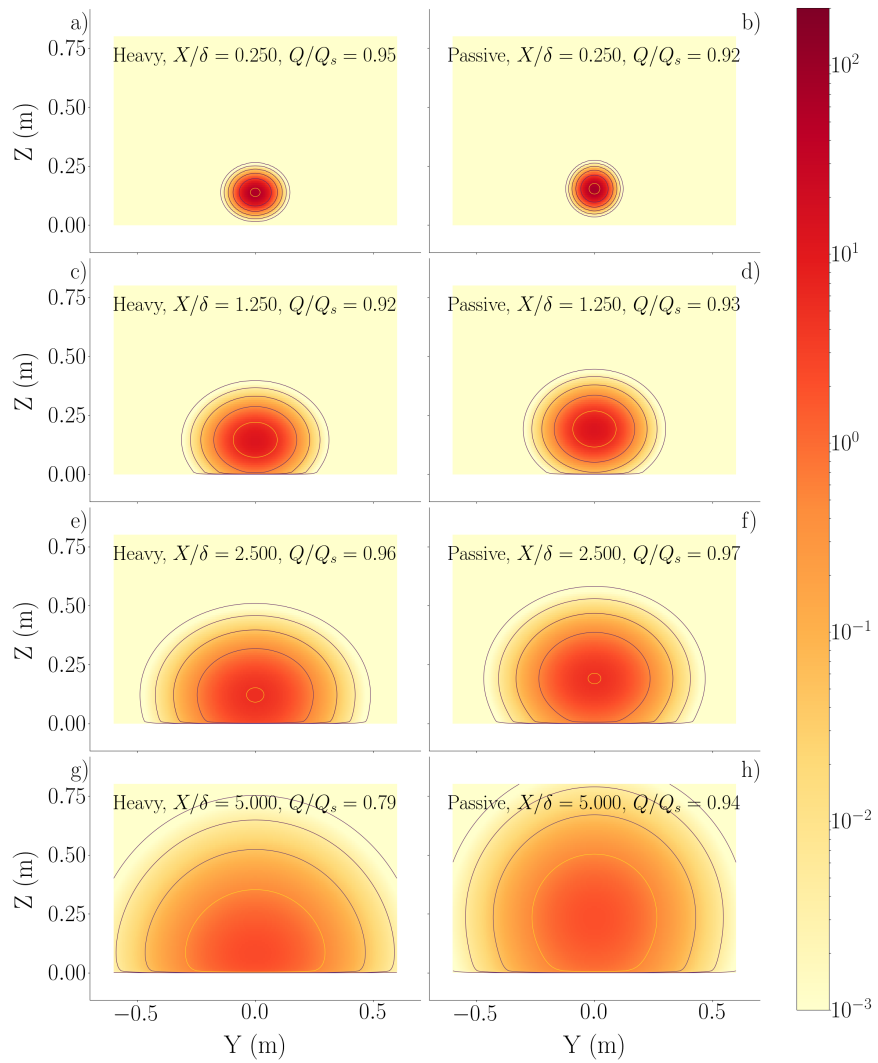


Figure 7: Mass fluxes in the cross-flow section for increasing section from the source for a), c), e), g), heavy gas and b), d), f), h), passive plume.

402 We measured the pollutant concentration field downwind the source and analysed the  
403 dimensionless mean concentration  $\bar{c}^*$ . This clearly showed the effect of buoyancy on  
404 the development of the heavy gas plume downwind the source. Simultaneous measure-  
405 ments of concentration and velocity allowed us to obtain vertical profiles of streamwise  
406 turbulent mass fluxes  $\overline{u'c'^*}$ . The distribution of the mass flux in the cross-flow sections  
407 enlightened the vertical displacement of the heavy gas plume, compared to the passive  
408 scalar, due to its negative buoyancy. The estimates of the longitudinal mean and turbu-  
409 lent mass fluxes allowed us to evaluate the total mass fluxes as  $\overline{uc^*} = \overline{u^*} \cdot \bar{c}^* + \overline{u'c'^*}$ . We  
410 integrated  $\overline{uc^*}$  in the cross-flow section of the plume at increasing distances from the  
411 source and we compared these values to the mass-flow rate provided by the flow-meter  
412 in order to verify the integral mass balance. We found that the differences were of about  
413 10% for both the passive scalar and the heavy density releases. This shows that the two  
414 sets of data have a similar accuracy and, therefore, the calibration process developed  
415 in this study provides measurements for a heavy gas plume that are as reliable as those  
416 obtained for a passive scalar plume.

#### 417 **Acknowledgements**

418 C. Vidali is funded by Air Liquide.

#### 419 **References**

- 420 [1] R. E. Britter, Atmospheric dispersion of dense gases, *Annual Review of Fluid*  
421 *Mechanics* 21 (1989) 317–344.
- 422 [2] R. N. Meroney, Guidelines for fluid modeling of dense gas cloud dispersion,  
423 *Journal of Hazardous Materials* 17 (1987) 23 – 46.
- 424 [3] G. Comte-Bellot, Hot-wire anemometry, *Annual Review of Fluid Mechanics* 8  
425 (1976) 209–231.
- 426 [4] R. L. Simpson, W. G. Wyatt, The behaviour of hot-film anemometers in gas  
427 mixtures, *Journal of Physics E: Scientific Instruments* 6 (1973) 981–987.

- 428 [5] D. T. Wasan, K. M. Baid, Measurement of velocity in gas mixtures: Hot-wire and  
429 hot-film anemometry, *AIChE Journal* 17 (1971) 729–731.
- 430 [6] W. M. Pitts, B. J. McCaffrey, Response behaviour of hot wires and films to flows  
431 of different gases, *Journal of Fluid Mechanics* 169 (1986) 465–512.
- 432 [7] A. Banerjee, M. J. Andrews, A convection heat transfer correlation for a binary  
433 air-helium mixture at low Reynolds number, *Journal of Heat Transfer* 129 (2007)  
434 1494–1505.
- 435 [8] J. Way, P. A. Libby, Hot-wire probes for measuring velocity and concentration in  
436 helium-air mixtures, *AIAA Journal* 8 (1970) 976–978.
- 437 [9] S. Corrsin, Extended applications of the hot-wire anemometer, *Review of Scien-  
438 tific Instruments* 18 (1947) 469–471.
- 439 [10] J. McQuaid, W. Wright, The response of a hot-wire anemometer in flows of gas  
440 mixtures, *International Journal of Heat and Mass Transfer* 16 (1973) 819 – 828.
- 441 [11] B. Talbot, N. Mazellier, B. Renou, L. Danaila, M. A. Boukhalfa, Time-resolved  
442 velocity and concentration measurements in variable-viscosity turbulent jet flow,  
443 *Experiments in Fluids* 47 (2009) 769.
- 444 [12] G. Zhu, S. Arya, W. H. Snyder, An experimental study of the flow structure within  
445 a dense gas plume, *Journal of Hazardous Materials* 62 (1998) 161 – 186.
- 446 [13] M. R. Raupach, B. J. Legg, Turbulent dispersion from an elevated line source:  
447 measurements of wind-concentration moments and budgets, *Journal of Fluid  
448 Mechanics* 136 (1983) 111–137.
- 449 [14] H. Stapountzis, B. L. Sawford, J. C. R. Hunt, R. E. Britter, Structure of the  
450 temperature field downwind of a line source in grid turbulence, *Journal of Fluid  
451 Mechanics* 165 (1986) 401–424.
- 452 [15] J. E. Fackrell, A. G. Robins, Concentration fluctuations and fluxes in plumes  
453 from point sources in a turbulent boundary layer, *Journal of Fluid Mechanics* 117  
454 (1982) 1–26.

- 455 [16] K. Koeltzsch, The height dependence of the turbulent Schmidt number within the  
456 boundary layer, *Atmospheric Environment* 34 (2000) 1147 – 1151.
- 457 [17] M. M. Metzger, J. C. Klewicki, Development and characterization of a probe  
458 to measure scalar transport, *Measurement Science and Technology* 14 (2003)  
459 1437–1448.
- 460 [18] K. M. Talluru, C. Hernandez-Silva, J. Philip, K. A. Chauhan, Measurements of  
461 scalar released from point sources in a turbulent boundary layer, *Measurement*  
462 *Science and Technology* 28 (2017) 055801.
- 463 [19] D. Contini, P. Hayden, A. Robins, Concentration field and turbulent fluxes during  
464 the mixing of two buoyant plumes, *Atmospheric Environment* 40 (2006) 7842 –  
465 7857.
- 466 [20] M. Carpentieri, A. G. Robins, Tracer flux balance at an urban canyon intersection,  
467 *Boundary-Layer Meteorology* 135 (2010) 229–242.
- 468 [21] M. Carpentieri, P. Hayden, A. G. Robins, Wind tunnel measurements of pollutant  
469 turbulent fluxes in urban intersections, *Atmospheric Environment* 46 (2012) 669  
470 – 674.
- 471 [22] J. Abbiss, T. Chubb, E. Pike, Laser Doppler anemometry, *Optics & Laser Tech-*  
472 *nology* 6 (1974) 249 – 261.
- 473 [23] M. Marro, H. Gamel, P. Méjean, H. Correia, L. Soulhac, P. Salizzoni, High-  
474 frequency simultaneous measurements of velocity and concentration within tur-  
475 bulent flows in wind-tunnel experiments, *Experiments in Fluids* 61 (2020) 245.
- 476 [24] E. Müller, H. Nobach, C. Tropea, A refined reconstruction-based correlation  
477 estimator for two-channel, non-coincidence laser Doppler anemometry, *Meas.*  
478 *Sci. Technol.* 9 (1998) 442–451.
- 479 [25] H. Nobach, Present methods to estimate the cross-correlation and cross-spectral  
480 density for two-channel laser Doppler anemometry, in: 18th International Sym-  
481 posium on the Application of Laser and Imaging Techniques to Fluid Mechanics,  
482 Lisbon, Portugal, 4–7 July, 2016.

- 483 [26] R. N. Meroney, Wind-tunnel experiments on dense gas dispersion, *Journal of*  
484 *Hazardous Materials* 6 (1982) 85 – 106.
- 485 [27] M. Schatzmann, W. H. Snyder, R. E. Lawson, Experiments with heavy gas jets  
486 in laminar and turbulent cross-flows, *Atmospheric Environment. Part A. General*  
487 *Topics* 27 (1993) 1105 – 1116.
- 488 [28] W. H. Snyder, Wind-tunnel study of entrainment in two-dimensional dense-gas  
489 plumes at the EPA's fluid modeling facility, *Atmospheric Environment* 35 (2001)  
490 2285 – 2304.
- 491 [29] G. Briggs, R. Britter, S. Hanna, J. Havens, A. Robins, W. Snyder, Dense gas verti-  
492 cal diffusion over rough surfaces and results of wind-tunnel studies, *Atmospheric*  
493 *Environment* 35 (2001) 2265–2284.
- 494 [30] S. R. Hanna, J. C. Chang, Use of the Kit Fox field data to analyze dense gas  
495 dispersion modeling issues, *Atmospheric Environment* 35 (2001) 2231 – 2242.
- 496 [31] R. E. Britter, W. H. Snyder, Fluid modeling of dense gas dispersion over a ramp,  
497 *Journal of Hazardous Materials* 18 (1988) 37 – 67.
- 498 [32] G. Briggs, R. E. Britter, S. R. Hanna, J. Havens, S. B. King, A. G. Robins, W. H.  
499 Snyder, K. W. Steinberg, *Advances in Dense Gas Dispersion Modeling of Ac-*  
500 *cidental Releases over Rough Surfaces during Stable Conditions*, Springer US,  
501 Boston, MA, 1998, pp. 509–516.
- 502 [33] A. Robins, I. Castro, P. Hayden, N. Steggel, D. Contini, D. Heist, A wind tunnel  
503 study of dense gas dispersion in a neutral boundary layer over a rough surface,  
504 *Atmospheric Environment* 35 (2001) 2243 – 2252.
- 505 [34] J. Donat, M. Schatzmann, Wind tunnel experiments of single-phase heavy gas  
506 jets released under various angles into turbulent cross flows, *Journal of Wind*  
507 *Engineering and Industrial Aerodynamics* 83 (1999) 361–370.
- 508 [35] A. Robins, M. Carpentieri, P. Hayden, J. Batten, J. Benson, A. Nunn, MODITIC  
509 wind tunnel experiments, in: *17th International Conference on Harmonisation*

- 510 within Atmospheric Dispersion Modelling for Regulatory Purposes, Budapest,  
511 Hungary, 9-12 May, 2016.
- 512 [36] G. Iacobello, M. Marro, L. Ridolfi, P. Salizzoni, S. Scarsoglio, Experimental  
513 investigation of vertical turbulent transport of a passive scalar in a boundary layer:  
514 Statistics and visibility graph analysis, *Phys. Rev. Fluids* 4 (2019) 104501.
- 515 [37] J. E. Fackrell, A flame ionisation detector for measuring fluctuating concentra-  
516 tion, *Journal of Physics E: Scientific Instruments* 13 (1980) 888.
- 517 [38] C. Nironi, P. Salizzoni, M. Marro, P. Mejean, N. Grosjean, L. Soulhac, Dispersion  
518 of a passive scalar fluctuating plume in a turbulent boundary layer. Part I: Velocity  
519 and concentration measurements, *Boundary-Layer Meteorology* 156 (2015) 415–  
520 446.
- 521 [39] C. Ltd., HFR400 - Fast Response Hydrocarbon Measurement System - User Man-  
522 ual, Technical Report, Cambustion Limited, 2006.
- 523 [40] D. T. Pritchard, J. A. Currie, Diffusion of coefficients of carbon dioxide, nitrous  
524 oxide, ethylene and ethane in air and their measurement, *Journal of Soil Science*  
525 33 (1982) 175–184.
- 526 [41] A. E. Perry, G. L. Morrison, A study of the constant-temperature hot-wire  
527 anemometer, *Journal of Fluid Mechanics* 47 (1971) 577–599.
- 528 [42] H. H. Bruun, Hot-wire anemometry: Principles and signal analysis, *Measurement*  
529 *Science and Technology* 7 (1996).
- 530 [43] F. E. Jorgensen, How to measure turbulence with hot-wire anemometers - a prac-  
531 tical guide, Technical Report, Dantec Dynamics, 2002.